Effect of Variation in Process Parameters on the Formation of Freckle in INCONEL 718 by Vacuum Arc Remelting

XIANHUI WANG, R. MARK WARD, MIKE H. JACOBS, and MARK D. BARRATT

In order to study the effect of variation in process parameters on the final ingot of INCONEL 718 during vacuum arc remelting, a 508-mm-diameter vacuum arc remelting (VAR) ingot of INCONEL 718 was produced under conditions of variation in electrode diameter and arc gap. It was sectioned and analyzed in the as-cast state. Freckle was found in the midradius and center regions when the electrode diameter and arc gap changed. The experimental results were discussed in relation to composition, current distribution, and fluid flow. Freckle formation was found to be associated with large changes in melting conditions probably resulting in significant perturbation of the fluid flow in the melt pool and mushy zone. Instability in the solidification process may contribute to the initiation and formation of freckle defects in INCONEL 718 ingot.

I. INTRODUCTION

DUE to their excellent properties in oxidation resistance, creep resistance, fatigue resistance, wear resistance, and strength at elevated temperatures, Ni-based superalloys are widely used in the key rotating parts of aircraft engines. Vacuum arc remelting (VAR) is an important secondary remelting process that is widely used for Ni-based superalloys to refine the structure, improve the cleanness, and reduce defects. The last is of great importance as the yield strength of Ni-based superalloys is increasingly sensitive to the presence of defects. Although improved control of melting processes has reduced the incidence of many melt-related defects (*e.g.*, freckles, solute-lean defects, or white spots),[1–9] such defects are still occasionally found in VAR material. During the past several decades, numerous improvements have been made through evolutionary design and melt shop practices. Many aspects of VAR have been evaluated extensively, for example, metal transfer, the relation of pool dimensions and ingot isotherms to heat balance, and the influence of melting rate on structure. The aim of the procedure is to produce a controlled, segregation-free ingot structure, but owing to metallurgical process complexity in the VAR process, some problems and precise mechanisms that govern the VAR process are still not completely clear. Up to now, the vacuum arc physics of the VAR furnace are only partially characterized, and the processing transients are not fully understood. Transients in the process conditions may affect process stability during VAR, thus fluid flow and solidification structures. The highest probability of generating solidification defects may occur during these process transients. At present, the application to larger diameter ingots with more rigorous quality standards is limited by this lack of understanding. Consequently, a deeper physical and metallurgical understanding of the effects of process conditions on the VAR process and the quality of the resulting ingot will be beneficial for manufacturers to predict optimum melting conditions and gain a better quality of VAR ingot with efficiency, capability, and reliability. This investigation is aimed at enhancing the fundamental understanding of the VAR process by experimental investigations on the structure in VAR ingot, produced in an industrial scale VAR furnace under varying process conditions.

II. EXPERIMENTAL METHOD

A 508-mm-diameter ingot of INCONEL* 718 pro-

---

*INCONEL is a trademark of Special Metals Corporation, Hereford, UK.

---

duced on an industrial-scale VAR furnace was examined. The major process parameters such as melting rate, current, voltage, drip short rates, etc. were recorded and monitored by the furnace control system (PLC). Also, a number of whole melting processes were videotaped. The electrode used for the VAR came from the primary vacuum induction melting process. The electrode had a nominal 420-mm diameter with a section of reduced (330-mm) diameter (this section was machined before melting) and was designed to remelt into a 508-mm-diameter ingot at a constant current under a constant

XIANHUI WANG is with the School of Materials Science and Engineering, Xi'an University of Technology, Xi'an 710048, People's Republic of China, and IRC in Materials for High Performance Application, The University of Birmingham, Birmingham B15 2TT, United Kingdom. Contact email: xhwang693@xaut.edu.cn R. MARK WARD, MIKE H. JACOBS, and MARK D. BARRATT, are with the IRC in Materials for High Performance Application, The University of Birmingham, Birmingham, B15 2TT, United Kingdom.

arc gap condition. When the melting reached the section of narrow diameter, the electrode was remelted at the same current. Unfortunately, the arc gap was not effectively controlled by the PLC when the melt zone went through this section due to unpredicted factors beforehand. During the entire process, the mold helium gas pressure was kept constant, approximately, at 0.5 kPa. The VAR ingot was cut into seven transverse sections. Each of these individual sections was cut longitudinally along the nominal ingot centerline, and then cut to produce about 20-mm-thick slices from the front faces of each of the seven sections. Each of these slices was again cut in half along its length to give two half slices from the left and right sides of the melt pool. The slices were then labeled from slice A1 (the bottom of the ingot) to slice A7 (the top of the ingot).

The left-hand slices were macroetched using acidic ferric chloride to reveal the grain structure. The right-hand slices were electrolytically etched in 50 pct HCl, followed by an electrolytic stain in 4 pct H_2SO_4, to reveal the macrosegregation features. Digital photography and flat-bed scanning were used to obtain images of the etched slices. Tree rings were used to determine the melt pool profile. On longitudinal sections of VAR ingots, tree rings appear as fragments of chains of equiaxed grains that decorate the solid/liquid interface and can be used to estimate the molten-pool shape.[10,11] The tree rings were observed by eye on the etched slices, varying the angle of incident light to distinguish each tree ring. The distribution of tree rings was manually mapped onto an overlaid transparent film and then digitized into a computer for further analysis. The microstructural observations were made on a LEITZ DM optical microscope using reflected light and digital imaging software. The same optical samples were used for scanning electron microscopy (SEM) observation and microsegregation measurements. The compositional analysis (as-polished samples) was conducted on a JEOL-6300 scanning electron microscope interfaced with a Link energy dispersive spectrometry (EDS) facility.

III. EXPERIMENTAL RESULTS

A. Macroscopic Characteristics of VAR Ingot

Figure 1 shows recorded process parameters, macrographs of slice 4 to slice 7, and molten pool profiles along with the length of the ingot that are overlaid on the longitudinal etched macroslices as the diameter of the electrode reduced from 420 to 330 mm and the arc gap irregularly varied. It can be seen from Figure 1 that as melting progressed to the narrow section of the electrode, the melt rate increased from initial 3.6 kg/min to approximately 5 kg/min and the arc gap increased to approximately 12 mm and then repeatedly fluctuated. The arc gap and melt rate continued to fluctuate throughout the narrow section of the electrode, although an overall trend could be observed on the melt rate, which decreased back toward its initial value. From the macrographs of grain and chemical etched slices A5 and A6, a pronounced change in both the ingot macrostructure and the melt pool shape can be seen, along with a large number of freckles and a transition from the columnar to equiaxed grains in the center region. From the evolution of the melt pool profiles along the length of the ingot during the section of narrow electrode, it can be found that the measured central pool depth increased from 200 to approximately 285 mm at the initial stage and then gradually decreased back to approximately 224 mm.

It is likely that the reduction in the electrode diameter and variation in arc gap affect electrical arc behavior and heat distribution atop the molten pool, which in turn affect the flow patterns and temperature distribution within the pool, alter the pool shape, and lead to the formation of freckles. The grain macrostructure and segregation-etched macrostructure of the longitudinal section are shown in Figure 2. Freckle lines or trails can be seen, which are apparent as segmented lines. In order to show freckle defects clearly, macrographs of local regions in F1 and F2 at higher magnification are shown in Figure 3. It can be observed that freckles have different morphologies at the midradius and central regions. Freckles at the midradius region have regular streak profiles, whereas these at the center region have irregular shape (the freckle is located above the white line, as labeled in Figure 3(b)). From the macrographs of the segregation-etched slices, it can be observed that freckles are normally generated at a significant distance from the chill region. Freckles are mostly found in the locations between the midradius and center of the ingot. Freckles in the midradius region of the ingot are almost at right angles to the columnar grains, but upon further observation, it can be found from Figure 4 that the freckle lines lie at an angle somewhat more horizontal than the tree rings outlining the pool shape. This finding is in agreement with observations made by Van Den Avyle et al.[12] Figure 5 shows the ingot exhibiting freckles in an almost quarter of transverse section in this VAR INCONEL 718 ingot. Once again, numerous dark freckle spots are visually observed in the center to midradius of the ingot. The average sizes of the freckle spots are of the order of millimeters.

B. Microscopic Characteristics of Freckles

1. Microstructure
Two regions marked by the dashed rectangles on the right side of slice A5 shown in Figure 6 were sectioned, polished/etched, and examined in order to reveal detailed features and the composition of freckle defects. The two regions will be referred to as "freckle 1" and "freckle 2." Figures 7 and 8 show SEM micrographs of freckles 1 and 2 at different magnifications, respectively. It shows the freckles in the as-cast ingot as a white streak with excessive heavy solute elements (niobium-rich regions appear bright in SEM images of INCONEL 718).

2. Freckle composition
The two polished but unetched freckle samples were analyzed by SEM/EDS. The compositions of freckles 1 and 2 and their surrounding matrix, with standard
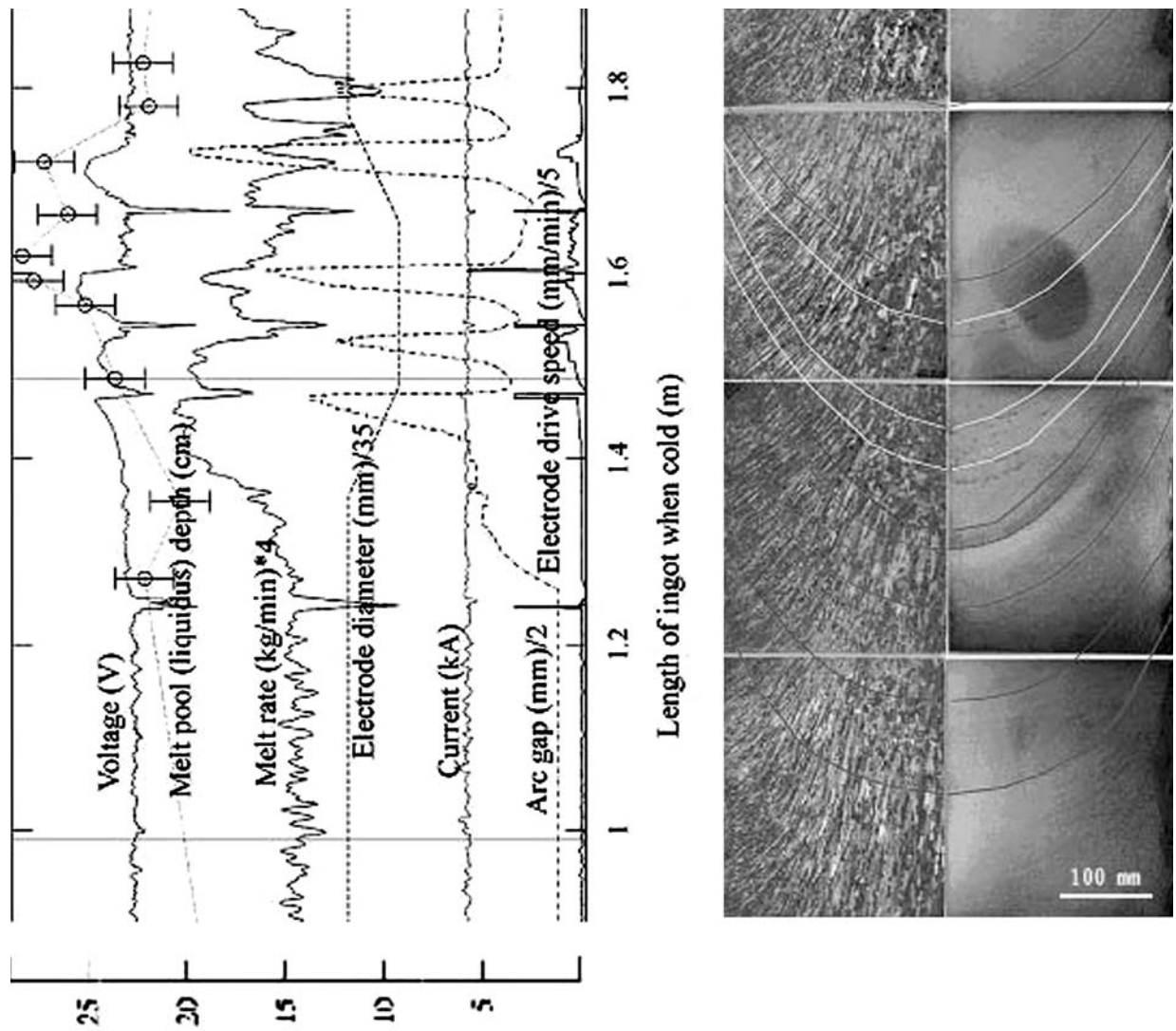
Fig. 1—Longitudinal cross sections A4, A5, A6, and A7 with process parameters.

deviations, are shown in Tables I and II, respectively. The results are the average compositions from the measured results at, at least five different locations. Significant compositional difference can be detected between the freckles and the matrix. The freckles are enriched with Nb, Mo, and Ti compared with the surrounding matrix. Among these elements, the segregation of Nb is the largest. In addition, it can be seen that the freckle 1 sample has an Nb content, which is approximately 90 pct higher than that of the freckle 2 sample.

IV. DISCUSSION

From Figure 1, it can be seen that the melt rate in narrow electrode/longer arc gap conditions is approximately 40 pct higher than that of the normal electrode/short arc gap condition. (The melt rate is highest in the narrow electrode experiment, because the electrode is just melting into the start of the narrow section.) The

increased melt rate definitely contributes to the volume of liquid in the melt pool and probably to the formation of freckles that are observed in this experiment, although it can be seen in Figure 1 that the freckles are actually formed when the melt rate is reducing from its peak. The results can be compared with the finding of the study by Morita et al.,[4] who conducted a trial in which a 380-mm-diameter electrode was melted into a 457-mm-diameter ingot. They found that freckles were generated when the melting rate increased by 50 pct (and the depth of the melt pool increased from 130 to 220 mm) as the current increased from 5.0 to 9.0 kA. Besides the melt rate, the fluid flow pattern within the liquid pool can influence the temperature distribution, the pool volume, and the final metallurgical structure. During the VAR process, there are two competing sources of motion in the melt pool: thermal buoyancy force and Lorentz force ($F = J \times B$). The surface of the melt pool is in contact with the electric arc and maybe 50 to 150 K above the melting point of the metal.[13] The large temperature difference will drive a buoyancy flow.
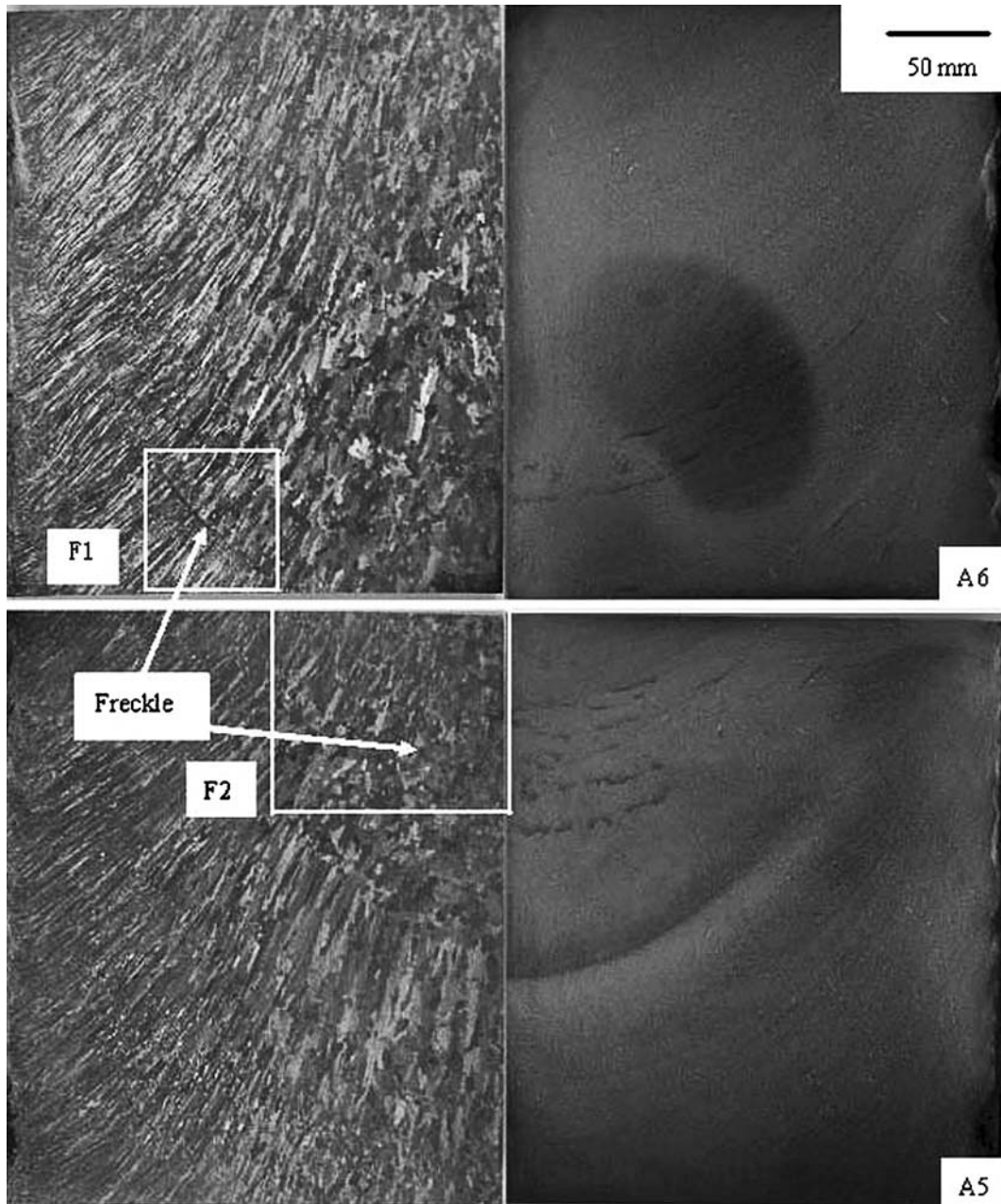
Fig. 2—Longitudinal macrostructures and macrosegregation structures of slices A5 and A6.

The second source of motion is the Lorentz force ($F = J \times B$), which arises from the flow of current through the pool. Figure 9 shows the two extreme cases: one in which buoyancy forces greatly outweigh the Lorentz force, and the other in which buoyancy forces may be neglected by comparison with Lorentz forces ($J \times B$). The difference of flow regimes between the thermal buoyancy forces and electromagnetic Lorentz forces has an important impact on the volume of the molten metal pool and macrosegregation formation tendency. When the thermal buoyancy forces are dominant, they tend to drive hot metal along the surface of the melt pool toward the edge and then down the sidewalls where a large amount of energy can be transferred to the crucible through the very thin chill zone and contact resistance. Therefore, thermal buoyancy forces will tend to decrease pool volume. On the other hand, when electromagnetic Lorentz forces are dominant, they bring the hot metal directly to the bottom of the liquid pool and hence tend to increase the liquid metal pool volume.

As the fluid flow is a very important factor to affect the ingot quality, a number of studies have been conducted through experimental observation and numerical simulation to decide what kind of current level results in fluid flow transition. Zanner et al.[14] reported a transition in fluid flow from buoyancy to Lorentz dominance as the melting current is increased from 6.6 to 7.6 kA. Bertram et al.[15] predicted the shape and size of the molten pool through modeling the VAR
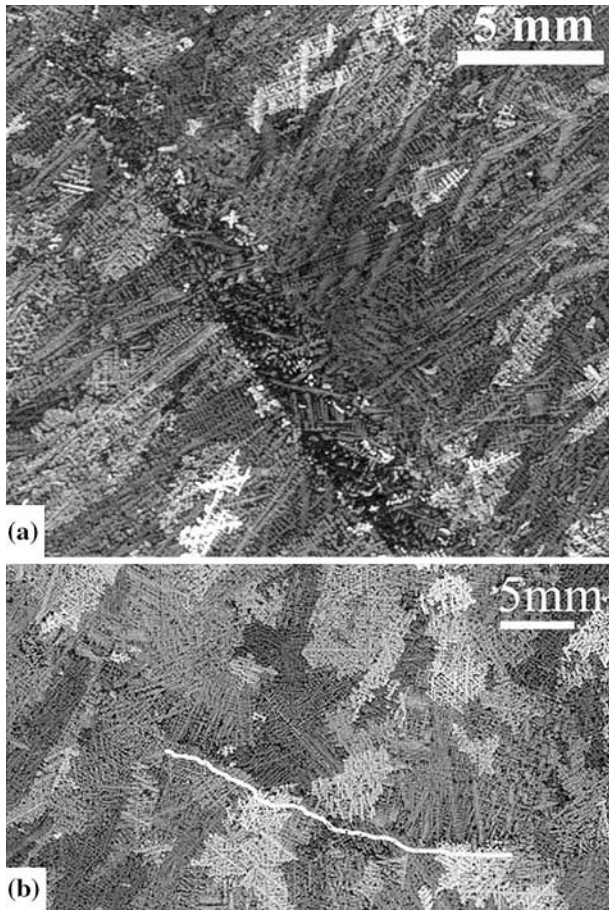
Fig. 3—Macrographs of freckle regions shown in Fig. 2 at higher magnifications: (*a*) F1 region and (*b*) F2 region (freckles are located above the white line).
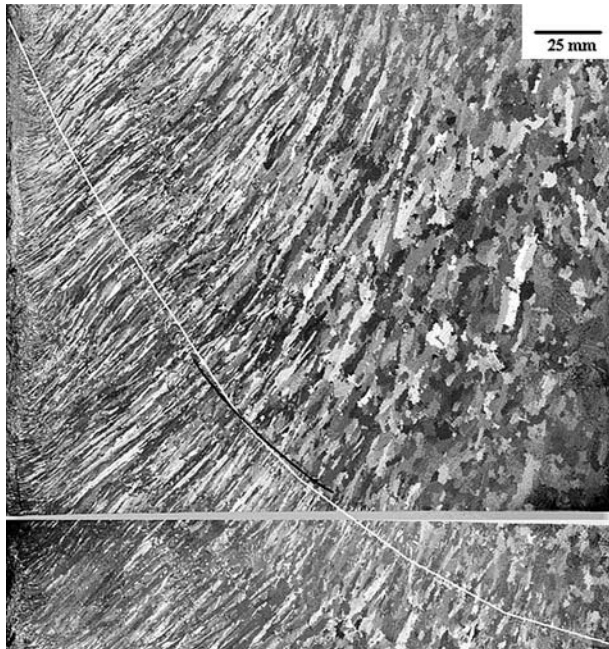

Fig. 4—Higher magnification view of freckle with melt pool shape overlaid (white line—melt pool shape, black line—freckle).
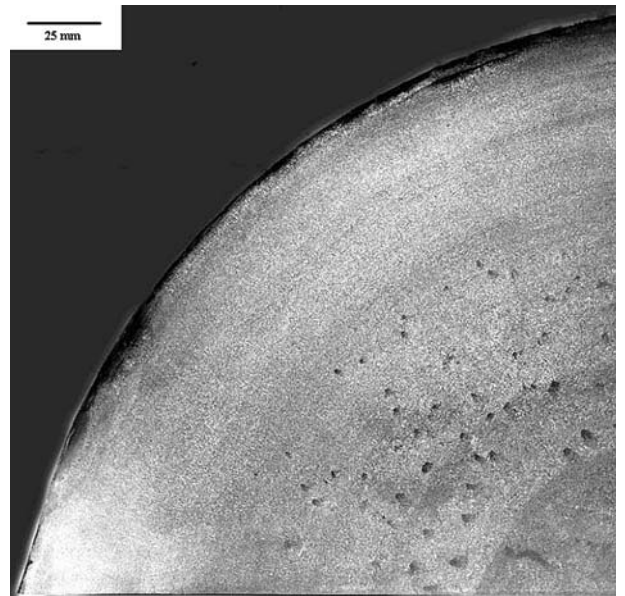

Fig. 5—Appearance of freckles in the transverse section.
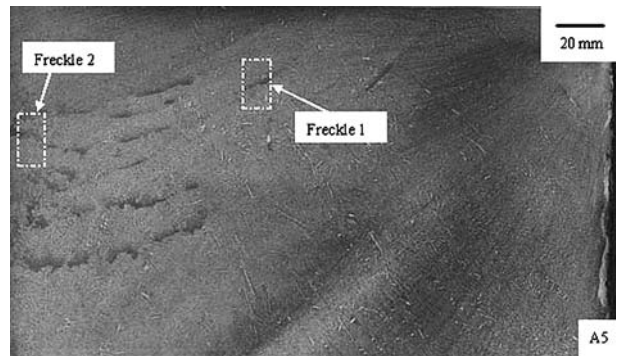

Fig. 6—Cutting-up locations of freckle samples.

of 508-mm-diameter ingots of INCONEL 718 at a number of casting rates and arc currents, with a two-dimensional axisymmetric quasi-steady-state approach. They found that, under the conditions in which VAR is normally used, the opposing buoyancy and Lorentz forces are very similar in magnitude and whichever is slightly dominant will tend to control the flow pattern. Numerical simulation results by Davidson *et al.*[16] predicted that there is a transition from buoyancy driven to current induced flow in the pool when the current is increased from 3.6 to 10.8 kA.

As discussed previously, it can be recognized that the magnitude of the current during VAR may influence the temperature distribution and fluid flow pattern in the melt pool. Therefore, it is significant to explore whether the change in current distribution within the ingot can alter the fluid flow and hence influence the depth of the melt pool and freckle formation.

As a part of the research project, the distribution of current entering the ingot and electrode from the crucible wall (at normal electrode/short arc gap and narrow electrode/longer arc gap conditions) was determined by Ward and Jacobs[17] using an indirect
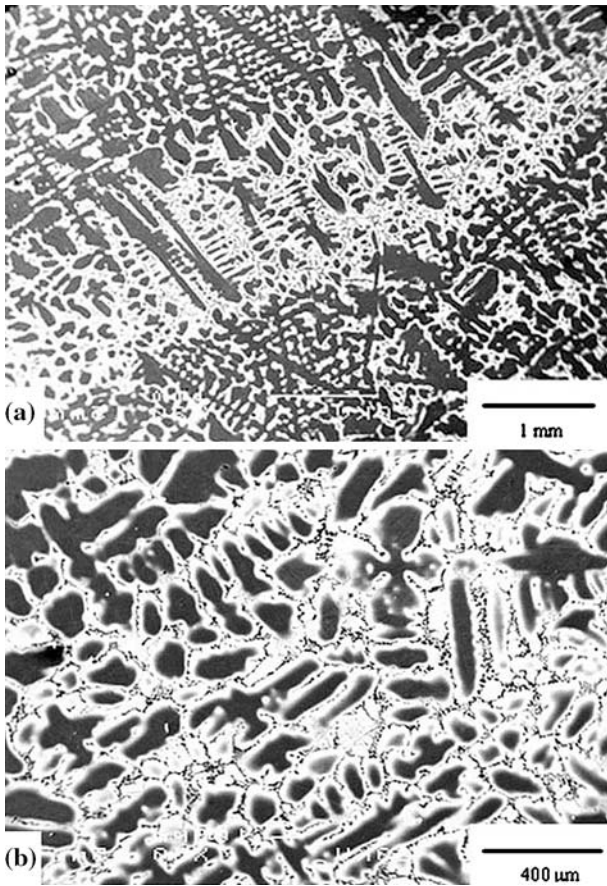
Fig. 7—SEM micrographs of freckle 1: (a) and (b) freckle 1 at different magnifications.
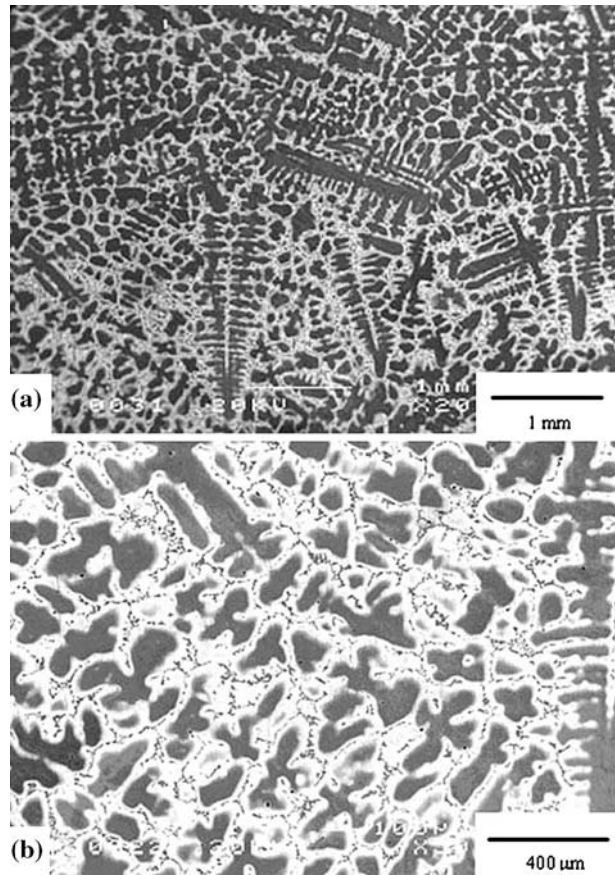

Fig. 8—SEM micrographs of freckle 2: (a) and (b) freckle 2 at different magnifications.

technique—the measurement of voltage gradients in the crucible wall. They found that the fraction of the total process current entering the ingot changes significantly when the electrode is narrowed. Approximately, 55 pct of the total melting current of 6 kA (*i.e.*, 3.3 kA) enters the ingot in the normal electrode/short arc gap condition, whereas approximately 73 pct of the total current (*i.e.*, 4.4 kA) enters the ingot produced in narrow electrode/longer arc gap conditions. Therefore, although the total current is maintained constant, the combined effect of the reduced electrode diameter and varied arc gap results in a larger fraction of the total current entering the ingot (which can be correlated to an increase in current density) as melting progresses to the narrow section of the electrode. The higher current density in this section leads to an increase in Lorentz forces. At present, it is still not clear whether this change can make Lorentz driven flow dominate and can produce a fully reversed fluid flow pattern. Even if this change could not lead to fully reversed fluid flow, the variation in the current entering the ingot undoubtedly enhances Lorentz driven flow. Therefore, the net effect is that the Lorentz driven flow partially counteracts buoyancy driven flow, and thus deepens the molten pool, which will tend to produce a larger mushy zone that may favor freckle formation. The results of simulation work by Evans[18] support the preceding

Table I. Compositions of Freckle 1 and the Surrounding Matrix Area (Weight Percent) with Standard Deviation

Element	Ti	Cr	Fe	Ni	Al	Nb	Mo	Si
Freckle 1	1.04	18.3	15.2	51.7	0.56	9.30	3.61	0.30
SD	0.11	0.83	0.94	1.10	0.14	2.50	0.31	0.12
Matrix	0.89	19.6	17.0	53.2	0.64	5.15	3.27	0.26
SD	0.09	0.30	0.40	0.16	0.05	0.44	0.10	0.04

Table II. Compositions of Freckle 2 and the Surrounding Matrix Area (Weight Percent) with Standard Deviation

Element	Ti	Cr	Fe	Ni	Al	Nb	Mo	Si
Freckle 2	1.08	18.8	15.8	53.1	0.63	7.10	3.32	0.23
SD	0.26	0.83	0.96	0.47	0.04	1.10	0.14	0.07
Matrix	0.90	19.5	17.0	53.1	0.59	5.48	3.25	0.24
SD	0.06	0.52	0.55	0.18	0.09	0.90	0.17	0.04

analysis. His simulation results for reasonable estimation of normal electrode and narrow electrode conditions show that the flow patterns change significantly, and the melt pool depth and mushy zone size apparently increase due to the change in current density and Lorentz force as the electrode diameter and arc focus are narrowed. Based on the preceding qualitative analysis, it
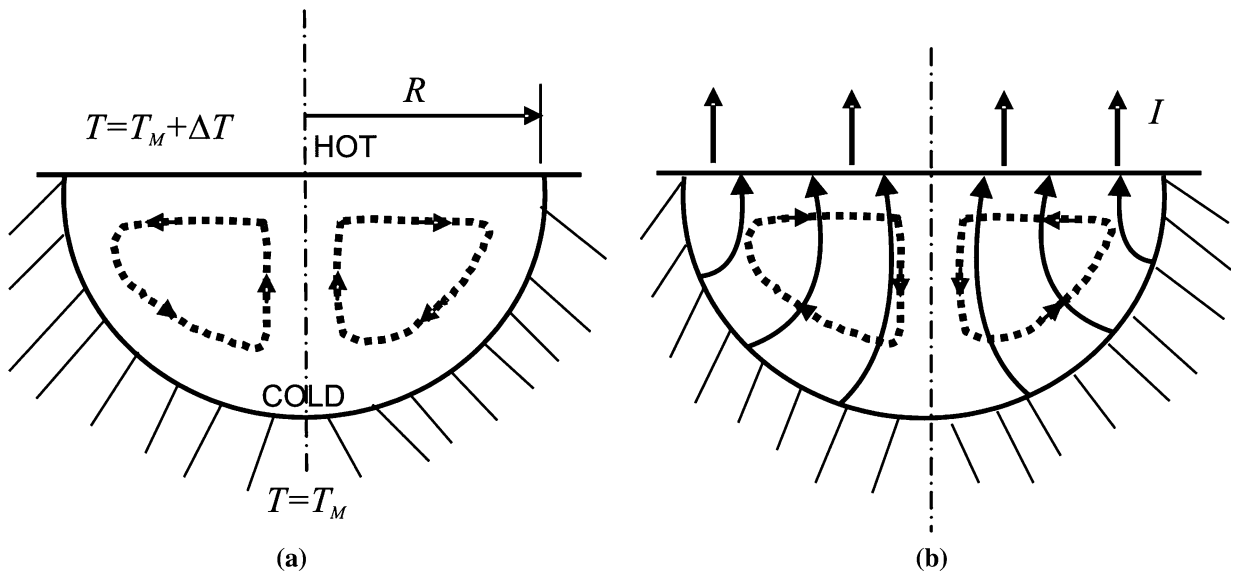
Fig. 9—Two extreme cases in vacuum arc remelting: (*a*) the Lorentz forces are neglected and (*b*) buoyancy forces are neglected. (The dashed lines indicate fluid flow, and the solid lines indicate current flow).

seems reasonable to conclude that when the electrode diameter is reduced, the molten pool becomes deeper owing to jointly contributory effects from the increase of melt rate and the change of current distribution.

It can be seen from Figures 1 and 2 that freckles are formed while the melt pool (at the section of narrow electrode) is deeper than that at normal electrode and arc gap conditions. It is interesting to note that freckles with different morphologies are found in columnar dendritic solidification structures (at midradius) and in equiaxed grain structures (in the central region), and their compositions are different. Because the low diffusion rate of niobium makes it virtually impossible to remove freckles by any kind of thermomechanical treatment in industry, it is significant to explore their formation mechanism so as to find ways to eliminate them at the remelting stage.

At present, it is generally believed that downward fluid flow within the mushy zone during solidification is responsible for the formation of freckles in the 718/625 superalloy VAR/ESR ingot.[12,19–20] A requirement for this type of channel defect to form is that the density of the interdendritic liquid increases during the solidification process. The other requirement is that the freckle grows into an increasing temperature field for a dissolution mechanism to occur and the channel to propagate. From the findings of experimental results, it is apparent that the first requirement is met. During solidification, the Nb, along with Mo and Ti, is rejected into the interdendritic area.[20–26] These elements influence the liquid density in different ways. Although the density of Nb at room temperatures is higher than that of INCONEL 718, the relationship between the density of the dendrite cores and that of the interdendritic liquid during solidification is complex. Although there is still some disagreement, it is currently believed that the interdendritic liquid becomes increasingly dense during the solidification of INCONEL 718.[12,20,27] However,

all of the alloying elements need to be included in the density calculations in order to show this effect. The Nb and C also control the precipitation of primary carbides. As the primary carbides precipitate, they remove both Nb and C from the liquid. As the solidification proceeds, the Nb-rich phases such as the δ (Ni$_3$Nb) and the Laves (Fe$_2$(Nb, Mo)) are formed from the Nb-rich interdendritic liquid in the later stage of solidification.[19,28,29] The second requirement is substantiated by the experimental results that freckle lines lie at an angle somewhat more horizontal than the molten pool profile determined by the tree rings (as seen in Figure 4). Attention is focused on three aspects of special interest in the following: (1) the effect of perturbations in the melt pool on the freckle formation tendency, (2) why the freckles are usually formed in the region between midradius and center, and (3) the freckle morphology within the equiaxed grain region at or near the center of the ingot.

The magnitude of fluid flow in the interdendritic regions depends strongly on the depth and profile of the melt pool, the mushy zone size, and the chemistry of the alloy. Yu and Flanders[11] demonstrated that a large mushy zone increases the chance of freckle formation. When the melt zone goes through the section of narrow diameter electrode in this investigation, the melt pool is deeper than that in normal electrode/arc gap conditions. This results in a larger mushy zone and steeper growth front angle, and thus enhances the intensity of solute-rich interdendritic fluid flow in the mushy zone during the solidification process. Possibly because of fluctuations in the arc gap in the section with a reduced diameter electrode, they could result in fluctuations in the fluid flow patterns, which could provide the driving force to initiate the formation of freckles.

From the experimental observations, it is found that freckles are located from the midradius to the central region. The results are consistent with the findings of

other authors.[2,12] The nature and extent of mushy zone defect formation are strongly influenced by the flow of solute-rich interdendritic liquid in the mushy zone and the depths of the melt pool during solidification. Flow of the interdendritic liquid is caused by solidification contraction, variation of fluid density, and electromagnetic force. However, the formation of freckles depends on not only the driving force derived from the density difference but also on the resistance to flow from the dendrites inside the mushy zone. Generally, the large melting rate results in a larger cooling rate and shorter local solidification time, i.e., deeper mushy zone and stronger interdendritic flow, and thus increases dendritic permeability and the probability for the freckle formation, but the formation of freckles is also related with the resistance to flow. During VAR solidification, high cooling rates at or close to the edge region produce much finer dendrite structure, and thus result in more resistance to suppress fluid flow. Subsequently, no freckles form in these outer regions. However, as the dendrite arm spacing in the region from midradius to center is sufficiently large, it will not impede fluid flow significantly. Therefore, freckles are typically found in the region from the midradius to the center. From Figure 6, freckles are observed to be discrete segments a few centimeters long on longitudinal samples; it is possible that these segments are, in fact, part of the same freckle, but because the freckle is crooked in three-dimensional (3-D) space, a planar section reveals discrete segments. However, it is very difficult to section the ingot to get a 3-D freckle morphology at this stage of investigation, so more research work is needed to determine freckle morphology in the future.

As seen in Figure 2, it should be noted that the macrostructure of slice A5 is equiaxed at the center in the region where the electrode diameter and arc gap change. The transition mechanism from columnar to equiaxed grains will not be discussed here in more detail, because it has been extensively studied over the years.[30–32] It is however interesting to speculate why the freckles found in the central region are different from those at the midradius.

From the observations, the freckle trails in the central equiaxed region have irregular shapes. It is of interest to explore the mechanism of their formation. As solidification progresses, elements such as Nb, Mo, and Ti are rejected into the surrounding interdendritic liquid. As the growing equiaxed grains impinge and intersect, they are surrounded by enriched solute liquid. Shrinkage also occurs due to the liquid/solid volume change. In this case, the fluid flow will be restricted due to the random nature of equiaxed grains, and it may be easier for the flow to follow the grain boundaries and forms the freckles with irregular shapes. In the narrow section, the higher melting rate results in deeper pools, which have the extended mushy zone and larger thermal gradients, and thus enhance flow in the interdendritic fluid. The precipitation of the Nb-rich phases results in an increase in liquid density during the solidification process of INCONEL 718, because there is a larger tilted growth front in the midradius region, and the permeability for fluid flow perpendicular to the mushy zone is 2.5 to 4 times greater than that for fluid flow parallel to the mushy zone;[33] the flow perpendicular to the direction of the dendrites is much easier than that parallel to the dendrites. Subsequently, flow of interdendritic liquid moves downward along the sloped pool profile. When interdendritic liquid flows into an increasing temperature field, they will dissolve some of the surrounding solute-lean solid,[12] and form the channel defect with regular streak profiles (as shown in Figure 3(a)). Therefore, freckle morphology in the equiaxed region is different from that in the columnar dendritic region.

In general, the freckle formation tendency is strongly influenced by density gradients in the solidifying mushy zone and resistance to flow. Increases in melt pool depth and mushy zone size as well as process instability favor freckle formation. The narrow diameter electrode and varying arc gap change the melting rate and current distribution in the ingot and are conducive to increase the depth of the melt pool. Although it is difficult to quantitatively determine which effect is larger at this stage of the research activity, the combined influence of the deep pool and perturbation in process conditions contributes to more interdendritic liquid flow that triggers the freckle formation. It is therefore recommended that the annular gap be selected carefully during the VAR process to minimize the chance of freckle formation.

At present, although the fluid flow and thermal fields may be characterized using numerical modeling reasonably well under steady-state conditions, the nature of process fluctuations could not be fully understood. Due to the aggressive environment during the VAR process, thermal parameters cannot be measured and some phenomena cannot be observed directly. It is suggested that a 3-D transient simulation of a complete remelting operation would contribute better understanding of the effects of the process conditions during steady state and transient furnace operating conditions, such as drip shorts and variation in arc gap on the fluid flow, solidification structure, and defect formation.

V. CONCLUSIONS

The main feature of the present work is to study the effect of variation in electrode diameter and arc gap on the structure of INCONEL 718 ingot. The results of the experimental investigation on slices A5 and A6 presented previously can be summarized as follows.

1. A large number of freckles are formed in a section of ingot produced when the electrode diameter and arc gap change. They are mostly located from the center to midradius of the as-cast ingot. The freckles show different morphologies in the midradius and center regions. Freckles in the midradius region have distinct streak profiles, whereas those in the center region have irregular shape.
2. Microstructural analysis shows that the freckles are a mixture of dendrites and heavily segregated interdendritic material. The freckles are enriched in niobium, molybdenum, and titanium compared with the matrix.

3. Freckle formation is found to be associated with large changes in melting conditions, which probably result in significant perturbation of the fluid flow in the melt pool and mushy zone. Instability in the solidification process may contribute to the initiation and formation of freckle defects in INCONEL 718 ingot.

ACKNOWLEDGMENTS

REFERENCES

1. G.E. Maurer: in *Superalloys, Supercomposites and Superceramics*, J.K. Tien and T. Caulfield, eds., Academic Press, Inc., San Diego, CA, 1989, pp. 49–80.
2. K.O. Yu, J.A. Domingue, G.E. Maurer, and H.D. Flanders: *JOM*, 1986, vol. 1, pp. 46–50.
3. K.O. Yu and J.A. Domingue: in *Superalloy 718—Metallurgy and Application*, E.A. Loria, ed., TMS, Warrendale, PA, 1989, pp. 33–48.
4. K. Morita, T. Suzuki, T. Taketsuru, D.G. Evans, and W. Yang: in *Superalloy 718, 625 706 and Derivatives*, E.A. Loria, ed., TMS, Warrendale, PA, 2001, pp. 149–60.
5. A. Mitchell: *Proc. Vacuum Melting Conf. on Specialty Metals Melting and Processing*, G.K Bhat and L.W. Lherbier, eds., TMS, Warrendale, PA, 1986, pp. 55–61.
6. L.A. Jackman, G.E. Maurer, and S. Widge: *Adv. Mater. Proc.*, 1993, vol. 5, pp. 18–25.
7. L.A. Jackman, G.E. Maurer, and S. Widge: in *Superalloys 718, 625, 706 and Various Derivatives*, E.A. Loria, ed., TMS, Warrendale, PA, 1994, pp. 153–61.
8. B.K. Damkroger, J.B. Kelley, M.E. Schlienger, J.A. Van Den Avyle, R.L. Williamson, and F.J. Zanner: in *Superalloys 718, 625 and Various Derivatives*, E.A. Loria, ed., TMS, Warrendale, PA, 1994, pp. 125–35.
9. X. Wang, M.D. Barratt, R.M. Ward, and M.H. Jacobs: *J. Mater. Sci.*, 2004, vol. 39, pp. 7169–74.
10. L.A. Bertram and F.J. Zanner: in *Modelling of Casting and Welding*, H.D. Brody and D. Apelian, eds., TMS-AIME, Warrendale, PA, 1980, pp. 333–49.
11. K.O. Yu and H.D. Flanders: *Proc. AVS Vacuum Arc Metallurgy Conf.*, G.K. Bhat and M. Lherbier, eds., AVS, Pittsburgh, PA, 1986, pp. 107–18.
12. J. Van Den Avyle, J.A. Brooks, and A.C. Powell: *JOM*, 1998, vol. 50 (3), pp. 22–25 49.
13. K.O. Yu: *Modelling for Casting and Solidification Processing*, Marcel Dekker, Inc., New York, NY, 2002, pp. 577–86.
14. F.J. Zanner, R.L. Williamson, R.P. Harrison, H.D. Flanders, R.D. Thompson, and W.C. Szeto: in *Superalloy 718—Metallurgy and Application*, E.A. Loria, ed., TMS, Warrendale, PA, 1989, pp. 17–32.
15. L.A. Bertram, C.B. Adasczik, D.G. Evans, R.S. Minisandram, P.A. Sackinger, D.D. Wegman, and R.L. Williamson: *Proc. 1997 Int. Symp. on Liquid Metal Processing and Casting*, A. Mitchell and P. Auburtin, eds., American Vacuum Society, Santa Fe, NM, 1997, pp. 110–32.
16. P.A. Davidson, X. He, and A.J. Lowe: *Mater. Sci. Technol.*, 2000, vol. 16, pp. 699–711.
17. R.M. Ward and M.H. Jacobs: *J. Mater. Sci.*, 2004, vol. 39, pp. 7135–43.
18. D.G. Evans: Special Metals Corporation, New Hartford, CT, unpublished research, 2004.
19. Y. Murata, M. Morinaga, N. Yukawa, H. Ogawa, and M. Kato: in *Superalloys 718, 625, 706 and Various Derivatives*, E.A. Loria, ed., TMS, Warrendale, PA, 1994, pp. 81–88.
20. W. Chen, W.H. Yang, K.M. Chang, S.K. Mannan, and J.J. DeBarbadillo: *Proc. 1999 Int. Symp. of Liquid Metal Processing and Casting*, A. Mitchell, L. Ridgway, and M. Baldwin, eds., AVS, Santa Fe, NM, 1999, pp. 122–29.
21. J.F. Radavich: in *Superalloy 718: Metallurgy and Applications*, E.A. Loria, ed., TMS, Warrendale, PA, 1989, pp. 229–40.
22. M.J. Cieslak, G.A. Knorovsky, T.J. Headley, and J.A.D. Romig: in *Superalloy 718—Metallurgy and Applications*, E.A. Loria, ed., TMS, Warrendale, PA, 1989, pp. 59–68.
23. R.G. Carlson, E. Ohio, and J.F. Radavich: in *Superalloy 718*, E.A. Loria, ed., TMS, Warrendale, PA, 1989, pp. 79–95.
24. G.A. Knorovsky, M.J. Cieslak, T.J. Headley, A.D. Romig, and W.F. Hammetter: *Metall. Mater. Trans. A*, 1989, vol. 20A, pp. 2149–60.
25. W. Yang, W. Chen, K.M. Chang, S. Manna, and J. DeBarbadillo: *Metall. Mater. Trans. A*, 2000, vol. 31A, pp. 2569–74.
26. W.H. Yang, W. Chen, K.M. Chang, S.K. Mannan, and J. DeBarbadillo: *9th Int. Symp. on Superalloys*, T.M. Pollock, R.D. Kissinger, R.R. Bowman, and K.A. Green, eds., TMS-AIME, New York, NY, 2000b, pp. 75–84.
27. A. Mitchell and T. Wang: in *Superalloy 718, 625 706 and Derivatives*, E.A. Loria, ed., TMS, Warrendale, PA, 2001, pp. 81–90.
28. M.J. Cieslak: *Weld. J.*, 1991, vol. 70, pp. 49–56.
29. K.M. Chang, H.J. Lai, and J.Y. Hwang: in *Superalloys 718, 625, 706 and Various Derivatives*, E.A. Loria, ed., TMS, Warrendale, PA, 1994, pp. 683–94.
30. H. Fredriksson and A. Olsson: *Mater. Sci. Technol.*, 1986, vol. 2, pp. 508–16.
31. S.C. Flood and J.D. Hunt: *Metals Handbook*, 9th ed., ASM INTERNATIONAL, Metals Park, OH, 1988, vol. 15, pp. 130–35.
32. A. Ghosh: *Sādhanā*, 2001, vol. 26, pp. 5–24.
33. P. Auburtin, T. Wang, S.L. Cockcroft, and A. Mitchell: *Metall. Mater. Trans. B*, 2000, vol. 31B, pp. 801–11.